



HAL
open science

A pavement-watering thermal model for SOLENE-microclimat: development and evaluation

Marie-Hélène Azam, Jérémy Bernard, Benjamin Morille, Marjorie Musy,
Hervé Andrieu

► **To cite this version:**

Marie-Hélène Azam, Jérémy Bernard, Benjamin Morille, Marjorie Musy, Hervé Andrieu. A pavement-watering thermal model for SOLENE-microclimat: development and evaluation. *Urban Climate*, 2018, 25, pp.22-36. 10.1016/j.uclim.2018.04.005 . hal-01790917v2

HAL Id: hal-01790917

<https://hal.science/hal-01790917v2>

Submitted on 31 May 2018

HAL is a multi-disciplinary open access archive for the deposit and dissemination of scientific research documents, whether they are published or not. The documents may come from teaching and research institutions in France or abroad, or from public or private research centers.

L'archive ouverte pluridisciplinaire **HAL**, est destinée au dépôt et à la diffusion de documents scientifiques de niveau recherche, publiés ou non, émanant des établissements d'enseignement et de recherche français ou étrangers, des laboratoires publics ou privés.

A pavement-watering thermal model for SOLENE-microclimat: development and evaluation

AZAM Marie-Hélène^{a,c,1,*}, BERNARD Jérémy^b, MORILLE Benjamin^a,
MUSY Marjorie^{a,c,1}, ANDRIEU Hervé^{a,d}

^a*Institut de Recherche en Sciences et Techniques de la Ville, FR CNRS 2488, F-44000
Nantes, France*

^b*UMR CNRS 6285, Lab-STICC, F-56000 Vannes, France*

^c*Cerema, F-44000 Nantes, France*

^d*Institut français des sciences et technologies des transports, de l'aménagement et des
réseaux, F-44000 Bouguenais, France*

^e*UMR CNRS 6183, GeM, Université de Nantes, F-44000 Nantes, France*

Abstract

In a dense urban area, pavement watering could be a solution to mitigate the Urban Heat Island. So far, mainly experimental studies have been used to evaluate watering techniques. In this study, a soil model dedicated to pavement watering has been developed within the urban climate model SOLENE-Microclimat. This watering model is presented and evaluated via a measurement campaign performed on an asphalt car park during warm days. The measurement campaign reveals that the surface cooling is mainly due to evaporation (80%). However, under warm conditions, the heat flux exchanged between the runoff water and the surface should also be modelled. Indeed, watering events are modelled through a runoff convective heat flux and a latent heat flux. The mean daily RMSE between estimated and observed surface temperature is 1.04°C, 0.86°C, 0.66°C, 0.35°C and 0.21°C

*Corresponding author. E-mail address: marie-helene.azam@cerema.fr Address: Cerema, 9 rue René Viviani, 44000 Nantes, France

respectively at the surface, 5 cm-, 10 cm-, 34 cm- and 50 cm-depths.

Keywords: Pavement-watering, Soil surface temperature,
SOLENE-Microclimat, Urban Heat Island, Climate Adaptation

Highlights

- A watering model is proposed to assess the impact of pavement watering techniques.
- Waterings are modelled by a runoff convective heat flux and a latent heat flux.
- Under warm conditions both fluxes should be modelled to reproduce the dynamics.
- Temperature observed at several depths are used to evaluate the computed temperature.

Contents

1	Introduction	5
1.1	Watering techniques	5
1.2	Pavement watering in microclimatic models	7
2	Method	9
2.1	SOLENE-microclimat soil model	9
2.2	Proposed watering model	11
2.2.1	Energy balance at the surface	11
2.2.2	Runoff convective heat flux	13
2.2.3	Latent heat flux between water and atmosphere	14
2.2.4	Heat fluxes dynamic	17
3	Model assessment	20
3.1	Case study	20
3.1.1	Studied area and measurement description	20
3.1.2	Description of the watering events	21
3.1.3	Validation of the model assumptions	23
3.1.4	Water budget	25
3.2	Comparison between simulation and measurement	26
3.2.1	Model setup	27
3.2.2	Watering model evaluation on ROSURE data	30
3.2.3	Model sensitivity to the discretization	33
4	Conclusion	36

1. Introduction

The Intergovernmental Panel on Climate Change (IPCC) assessed that heatwaves will be more frequent and more intense during the 21st century than during the 20th century. The last major European heatwaves led to approximately 70,000 excess deaths across the continent (Robine et al., 2008 [1]). The urban heat island (UHI) effect exacerbates the consequences of such climatic event on human health, as confirmed by Laaidi et al. (2012 [2]) and Conti et al. (2005 [3]) who showed a clear relationship between UHI and mortality in Paris and in Italian cities respectively. Reducing the UHI is then a major challenge addressed to the scientific community. Several countermeasures are currently investigated in all regions of the world and under different climates. Santamouris et al. (2016 [4]) reviewed the performances of the most common UHI mitigation technologies: building material albedo, vegetation, water. He concludes that UHI may be partly or fully annihilated using a combination of all technologies but that there is a need to improve the performances of each of them. The present article focuses on the pavement watering solutions. Regardless the technique used to spread the water (cleaning trucks - Hendel et al., 2015 [5] - or sprinklers set in the street structure - Himeno et al., 2010 [6]), the correct modelling of the physical phenomenon induced by this technique and their interaction with local climate will help to improve its performances.

1.1. Watering techniques

In very dense urban areas, the UHI may be mitigated by spreading water over pavements. The evaporation of the water in the air and the heat flux

25 exchanged between the water and the ground contribute to cool both the sur-
26 face and the air temperature. It also induces an increase of the air humidity.
27 Yang and Zhao (2015 [7]) investigated the effect of different surfaces (water
28 ponds, low vegetation, asphalt) on the air temperature and humidity through
29 an experimental work realised under hot climate conditions. They measured
30 humidity and air temperature gradients over the different studied surfaces.
31 If they can measure high differences over the specific humidity variable close
32 to the ground, these differences strongly decrease with the height. At 1.2m
33 high, the profiles are similar, even with low air velocities. As a result, impact
34 of watering on air humidity should not alter the effect obtained thanks to
35 the lower surface temperature.

36 Daniel et al.(2016 [8]), confirmed that watering mainly limits the warming
37 of the urban surface, reducing their infrared emissions. They found that wa-
38 tering techniques have a positive impact on human comfort. The used index
39 comfort (UTCI) may be increased by the humidity but it is also decreased by
40 the air temperature and mainly by the surface temperature. Finally Broad-
41 bent at al. (2017 [9]) showed that the average increase of vapour pressure
42 did not have a negative influence on comfort under very hot and dry climate
43 (South Australia during summer).

44 Under warm conditions, these processes offer a quick response while the
45 water is spread over the surface. However, evaporation is constrained by the
46 pavement water-holding capacity (which depends on the surface roughness).
47 Below a certain volume of water spread, all the water is stored in the surface
48 porosity and can evaporate. Above a threshold proper to the surface char-

49 acteristics, the holding capacity of the surface is over-passed and the water
50 excess runs off toward sewers.

51 Watering techniques have been mainly studied through experimental works
52 (Hendel et al., 2015 [5], Himeno et al., 2010 [6]) which confirm the positive im-
53 pact of watering techniques. Himeno et al., (2010 [6]) found that in the case of
54 hot weather (above 30°C), pavement watering can reduce the air temperature
55 by 2°C in the morning and 4°C in the afternoon. Hendel et al. (2015 [10])
56 worked on the optimisation of those waterings, minimising the total amount
57 of water spread, maximising the evaporation. With a watering rate of 0.31
58 to 0.41L/m²/h every 30 minutes, the surface temperature could be reduced
59 by 4°C in the morning and 13°C in the afternoon. According to Broadbent
60 et al. (2017 [9]), the performance assessment of watering techniques during
61 heatwave conditions at the micro-scale has rarely been modelled. Daniel et
62 al. (2016 [8]), Grossman-Clarke et al. (2010 [11]) and Boadbent et al. (2017
63 [9]) evaluated the mitigation potential of these techniques at the meso-scale.

64 1.2. Pavement watering in microclimatic models

65 In the literature, most of the models used to simulate the urban sur-
66 face energy balance, calculate the latent heat flux induced by the vegetation
67 (Grimmond et al., 2010 [12]). However, these models are not appropriate
68 for pavement watering application since they do not consider the heat flux
69 exchanged between the surface and the runoff water.

70 The Town Energy Balance (TEB) model (Masson, 2000 [13]) is one of
71 the few urban climate models that is able to simulate pavement watering
72 events (Daniel et al., 2016 [8], Broadbent et al. 2017 [9]) at meso-scale. It

73 distinguishes the evapotranspiration from the evaporation over impervious
74 surfaces. In the case of impervious surface, the following processes are mod-
75 elled: interception, evaporation of the available water and surface runoff. For
76 each surface, a water reservoir is set according to the water holding capacity
77 of the pavement and its content is updated at each time step. It is filled dur-
78 ing a watering event and emptied by the evaporation. When the maximum
79 capacity of the reservoir is reached, the excess is transferred to the sewer.
80 By default, the pavement considered in the model is a road and its storage
81 capacity is set at 1mm (Daniel et al., 2016 [8]). However, this parameter is
82 a variable of the model and then may be set to a different value (see section
83 3.2.1).

84 The main purpose of this article is to present and evaluate a watering
85 model that has been developed within the SOLENE-Microclimat model. This
86 microclimatic model is a research tool dedicated to urban climate modelling
87 at the neighbourhood scale. It consists of several model pieces including
88 a radiative model SOLENE, and several urban surfaces models (buildings,
89 soils, vegetation...) which have been described and assessed in (Malys, 2012
90 [14]; Musy et al., 2015 [15]; Bouyer, 2009 [16]). In this tool as in most of the
91 microclimate tools (Grimmond et al., 2010 [12]), waterings over impervious
92 surface could not be model.

93 The watering model is elaborated based on a review of the literature and
94 evaluated on an open asphalt parking lot, chosen to avoid interference with
95 other surfaces thermal behaviour, like solar radiation diffusion and reflection
96 as well as long-wave emission from the surrounding vertical surfaces (building

97 facades). In these conditions, we can isolate the watering model from the
98 other SOLENE-microclimat model pieces and assess it properly. This article
99 is the second step of a complete evaluation of SOLENE-Microclimat soil
100 model. Indeed in a previous article (Azam et al., 2017 [17]), the soil model
101 has been assessed under same conditions.

102 The model is presented in section 2. After a review of the different meth-
103 ods used to calculate each heat flux, the model equations are developed and
104 the algorithm is sum-up in a flow-chart (section 2.2.4). Section 3 deals with
105 the model evaluation. The case study is first presented (section 3.1). Based
106 on those results assumptions previously made are verified. Results of the
107 model are compared to the observed temperature and heat flux (section 3.2).
108 The model is evaluated on surface temperature and latent heat flux. Finally,
109 the sensitivity of the model to the soil model node distribution is studied.

110 **2. Method**

111 The proposed watering pavement model will be an additional model pieces
112 to the soil model used in SOLENE-microclimat. The SOLENE-microclimat
113 original soil model is briefly presented in section 2.1 but further details are
114 available in Azam et al.(2017 [17]). Then the proposed watering model is
115 presented in section 2.2.

116 *2.1. SOLENE-microclimat soil model*

117 SOLENE-microclimat soil model is designed for an impervious surface
118 like a pavement coating. Only heat transfer is therefore taken into account,

119 the moisture transfer being neglected. The soil model is defined as a one-
 120 dimensional soil column (for each soil facet) where each layer has its own
 121 characteristics (Figure 1)

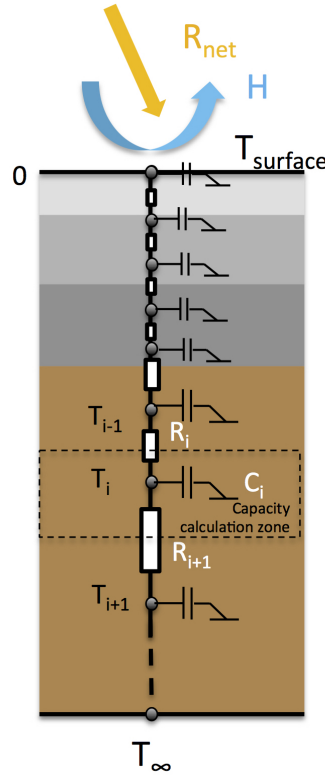


Figure 1: Schematic representation of the soil model: representation of the node distribution, heat resistances and capacities, description of a common cross-section of urban soil column with diffusive materials layers in shade of grey and underneath natural soil in brown (Azam et al., 2017 [17])

122 The problem is solved by a finite difference method using an electrical
 123 analogy. A mesh with one node per centimetre is used. At the surface,
 124 the upper boundary condition is defined by the surface energy balance detail
 125 after. The temperature at 0.75m is set with the measured temperature signal

126 at this depth. A more detailed description of the SOLENE-microclimat soil
127 model can be found in Azam et al. (2017 [17]).

128 *2.2. Proposed watering model*

129 *2.2.1. Energy balance at the surface*

130 The net radiative heat flux density (R_{net}) that reaches a dry pavement is
131 turned into two fluxes: a conductive heat flux density (Q_{cond}) and a sensible
132 heat flux density (H). Equation (1) is used to define the upper boundary
133 condition of the soil model.

$$R_{net} = Q_{cond} + H \quad (1)$$

134

135 R_{net} : net radiative heat flux density [W/m^2]

136 Q_{cond} : conductive heat flux density [W/m^2]

137 H : sensible heat flux density [W/m^2]

138

139 A watering event alters this energy balance. The water spread on a surface
140 follows one of the following path: 1/ infiltration in the soil, 2/run-off toward
141 the neighbouring surface or to the water network and 3/evaporation. Each
142 path implies a modification of the surface energy balance:

- 143 • a part of the water infiltrates the soil: the thermal properties of the soil
144 can vary with the water content and a heat flux is exchanged between
145 the water and the soil layers.
- 146 • a part of the water runs-off: a heat flux is exchanged between the water
147 and the surface.

148 • a part of the water evaporates: a latent heat flux is exchanged between
149 the water and the atmosphere.

150 Pavement surfaces can be modelled as semi-impervious surfaces (Dupont et
151 al., 2006 [18]) or as impervious surfaces (Herb et al., 2008 [19]; Hendel et
152 al., 2015 [10]). In the first case, downward infiltration should be taken into
153 account whereas the proportion of infiltrated water in the second case is
154 supposed negligible compared with the one that runs-off or evaporates. As
155 the model is only dedicate to paved surface (i.e. asphalt), we will consider our
156 surface as impervious. Overall the watering model needs to take into account
157 two fluxes initially not considered in Equation (1): a runoff convective heat
158 flux density exchanged between the surface and the water ($Q_{wat-pav}$) and a
159 latent heat flux density (LE) between the water and the atmosphere (Herb et
160 al., 2008 [19]; Hendel et al., 2015 [10]). The resulting surface energy balance
161 is then given by Equation (2). The calculation of these fluxes is further
162 described in the following sections.

$$R_{net} = Q_{cond} + H + Q_{wat-pav} + LE \quad (2)$$

163

164 LE : latent heat flux density exchanged between the water and the atmo-
165 sphere [W/m^2]

166 $Q_{wat-pav}$: runoff convective heat flux density exchanged between the surface
167 and the water [W/m^2]

168

169 *2.2.2. Runoff convective heat flux*

170 Herb et al. (2008 [19]) evaluated the convective heat flux exchanged
171 between the surface and the water from the energy absorbed by the water and
172 released by the soil. With the same idea, in our model, this runoff convective
173 flux is calculated from the energy absorbed by the water (Equation (3)). The
174 temperature variation is calculated between the soil surface temperature at
175 the time step t and the temperature of the water before it reaches the ground.
176 Herb et al. (2008 [19]) modelled rain events, the water temperature is then
177 supposed equal to the dew-point temperature. In our case, the water spread
178 is assumed equal to the pipe network temperature.

$$Q_{wat-pav} = \frac{\rho_w \cdot C_{p,w} \cdot h_{w,spr}}{\Delta t} (T_{surf}(t) - T_w) \quad (3)$$

179

180 $h_{w,spr}$: water height evenly sprinkled on the surface [m]

181 T_w : temperature of the water [K]

182 ρ_w : water density [kg/m^3]

183 $C_{p,w}$: water specific heat [$J/kg/K$]

184 $T_{surf}(t)$: surface temperature at the time step t [$J/kg/K$]

185

186 Herb et al. (2008 [19]) made the assumption that the runoff water reaches
187 the ground temperature instantly by conduction. The same assumption will
188 be made in the model and verified from the measurements analysis in section
189 3.1.3.

190 *2.2.3. Latent heat flux between water and atmosphere*

191 The evaporation is driven by two factors: the amount of heat available
192 at the free surface and the vapour pressure gradient in the near air. These
193 factors depend on meteorological variables including radiation, air pressure,
194 wind speed, temperature but also on other variables like the surface rough-
195 ness. Various methods have been developed to evaluate the evaporation rate.
196 Xu and Singh (1997 [20]; 2001 [21]) proposed to sort them into 6 classes: (i)
197 water budget, (ii) mass-transfer or aerodynamic based method, (iii) energy
198 budget method or combination (e.g. Penman, 1948), (iv) radiation, (v) tem-
199 perature based method, (vi) empirical methods. The empirical methods are
200 applicable only for specific cases with a specific range of variables, which
201 limits their application conditions. The radiation and the temperature based
202 methods are specific empirical methods. They only use one meteorological
203 variables as inputs (either radiation term, either temperature) to estimate
204 the evaporation whereas it is influenced by numerous other important fac-
205 tors (i.e. relative humidity, wind speed, etc). Singh and Xu (1997 [20])
206 observed that water budget method is based on a simple theoretical basis
207 but that they rarely produce reliable results. Energy budget method and
208 combination method reproduce well the physics but they need many meteo-
209 rological input data. Mass-transfer method is a good compromise since the
210 accuracy is reasonable (Singh and Xu, 1997 [20]) for less meteorological input
211 data needed. It is the most commonly used method to develop soil models
212 (Asaeda and Ca, 1993 [22]; Qin et al., 2002 [23]; Saito and Simunek, 2009
213 [24]; Herb et al., 2008 [19], Best, 1998 [25]). It is also used in our model.

214 The mass-transfer method is based on the Dalton Equation, described by

215 Equation (4).

$$LE = C \cdot [q_{sat}(T_{surf}) - q_a(T_{air})] \quad (4)$$

216

217 C : the aerodynamic conductance

218 $q_{sat}(T_{surf}) - q_a(T_{air})$: the vapour pressure gradient between the actual air
219 vapour pressure and the saturation vapour pressure at the surface tempera-
220 ture

221

222 The aerodynamic conductance is generally modelled using a combination
223 of the air density ρ_{air} , the latent heat L , and a heat transfer resistance R
224 (Equation (5)). Several methods can be used to calculate this last parameter.
225 The heat transfer resistance can be calculated as a function of the convective
226 heat transfer coefficient h_c (Mihalakakou et al. 1997 [26]; Herb et al., 2008
227 [19]); or as a combination of a surface and an aerodynamic resistance cal-
228 culated using standard Monin-Obukhov similarity theory (Best, 1998 [25];
229 Asaeda and Ca, 1993 [22]; Qin et al., 2002 [23]; Saito and Simunek, 2009
230 [24]).

$$C = \rho_{air} \cdot \frac{L}{R} \quad (5)$$

231

232 ρ_{air} : air density [kg/m^3]

233 L : the latent heat [J/kg]

234 R : heat transfer resistance's [s/m]

235

236 In our model, the heat transfer resistance is a function of the convective
237 heat transfer coefficient (Equation (6)). It is calculated from the correlation
238 method with a characteristic length of 1m (for more detail see Azam et al.,
239 2017 [17]). This method considers forced, mixed and natural convective heat
240 fluxes.

$$R = \rho_{air} \cdot \frac{C_{p,air}}{h_c} \quad (6)$$

241

242 $C_{p,air}$: air specific heat [$J/kg/K$]

243 h_c : the convective heat transfer coefficient [$W/m^2/K$]

244

245 As the surface is impervious, the latent heat flux is only calculated when
246 some water is present on the surface. This heat flux depends on the air char-
247 acteristics (temperature, pressure, humidity and wind speed). The vapour
248 pressure gradient is calculated between the air at a certain height and the
249 saturated air very close to the water surface. The hypothesis is made that
250 the saturated air very close to the water surface is at the same temperature
251 than the water surface. The vapour pressure is calculated according to the
252 Magnus-Tetens formulas (Alduchov and Eskridge, 1996 [27]) described by
253 Equations (7), (8) and (9).

$$q_{sat} = 0.662 \frac{VP_{sat}}{101325 - 0.378 VP_{sat}} \quad (7)$$

$$q_a = 0.662 \frac{VP_{sat} \frac{RH}{100}}{101325 - 0.378 VP_{sat} \frac{RH}{100}} \quad (8)$$

$$VP_{sat} = 611.2 \exp\left(\frac{17.67 T}{243.5 + T}\right) \quad (9)$$

254 VP_{sat} : saturated vapour pressure [Pa]

255 RH : Relative Humidity [%]

256

257 2.2.4. Heat fluxes dynamic

258 The Surface Energy Balance (hereafter denoted SEB) method is presented
 259 in Figure 2. For each time step, the equivalent height of water that is evenly
 260 sprinkled on the surface is noted $h_{w,spr}$. The total height of water is noted
 261 $h_{w,tot}$. Then three cases are considered:

- 262 • $h_{w,tot}$ is equal to 0,
- 263 • $h_{w,tot}$ is higher than 0 and $h_{w,spr}$ is higher than 0,
- 264 • or $h_{w,tot}$ is higher than 0 but $h_{w,spr}$ is equal to 0.

265 In the first case, the surface is dry then the conductive flux is simply de-
 266 fined as the difference between the global radiation flux and the sensible heat
 267 flux. In the second case, water is sprinkled on the surface. We assume that
 268 no evaporation occurs at this time step. The energy is exchanged between
 269 the water and the ground. This convective heat flux is calculated consid-
 270 ering that the additional height of water $h_{w,spr}$ reaches directly the surface
 271 temperature. Then a proportion of the total water height runs off decreasing
 272 the height of the water layer. The height $h_{w,cap}$ of the water layer that re-
 273 mains at the surface depends on the water-holding capacity of the pavement.
 274 In the third case, the sprinklers are off some water remains on the surface.

275 Only evaporation occurs and its potential is estimated and converted into
276 an equivalent water height $h_{evap,th}$. If $h_{w,tot}$ is higher than $h_{evap,th}$, the latent
277 heat flux is equal to the evaporation potential. The remaining height $h_{w,tot}$
278 is converted to an equivalent latent heat flux. The water height decrease is
279 equal to the evaporated water height. Then the next time step is considered.

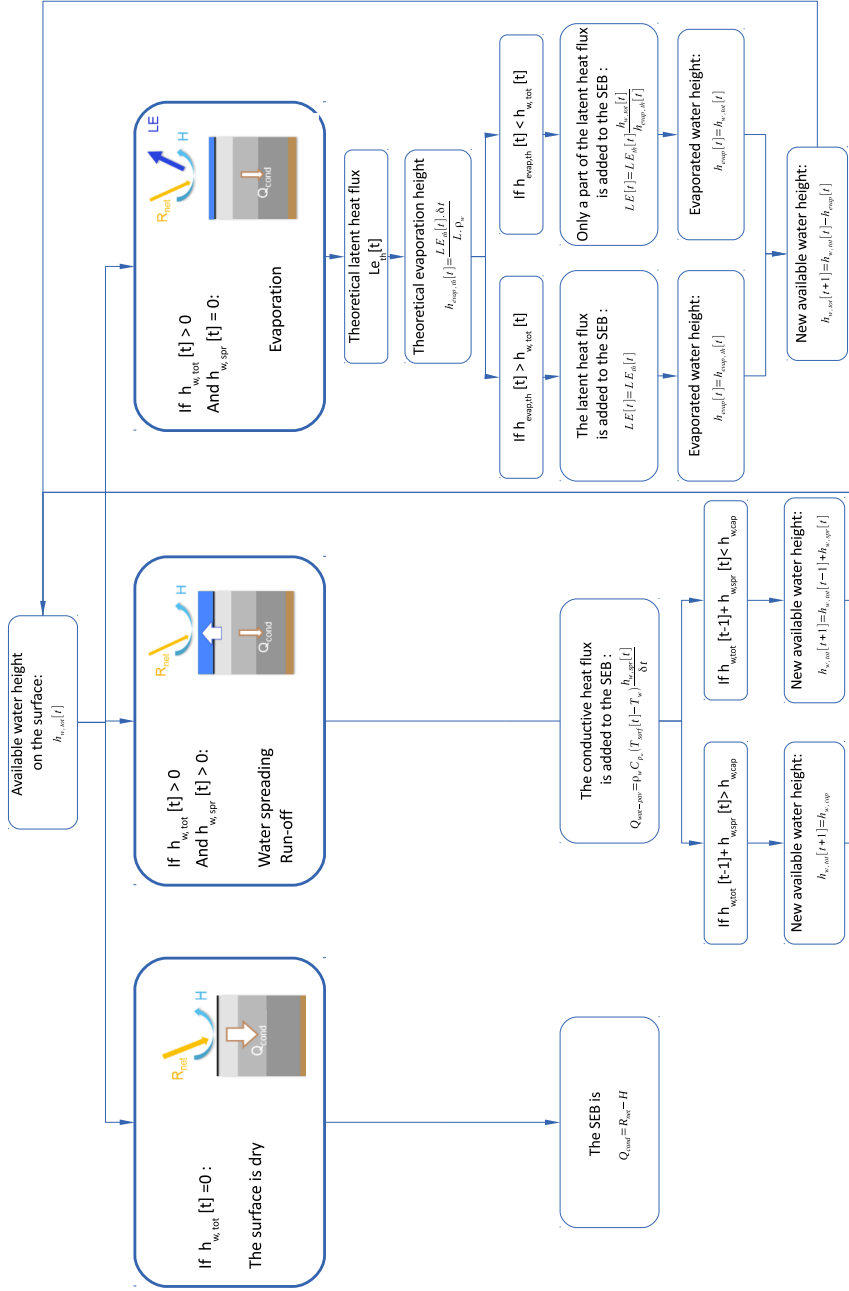


Figure 2: Flowchart of the surface energy balance calculation process for each step of a watering event

280 **3. Model assessment**

281 The model is evaluated on an open asphalt parking lot. The experiment
282 and the analysis of the watering event are presented in section 3.1. Then the
283 model will be applied to this case and assessed (section 3.2).

284 *3.1. Case study*

285 *3.1.1. Studied area and measurement description*

286 Data from the ROSURE/HydroVille experiment (Cohard et al., 2017
287 [28]) are used to calibrate and evaluate the pavement watering model. The
288 experiment site is located near Nantes (France) and consisted of an asphalt
289 car park of $2500m^2$. This experiment focused on surface and air temperatures
290 and on heat flux measurement during a warm summer period (June 2004).
291 The car park was watered by means of a set of artificial rain events (Figure
292 3).



Figure 3: View of the experimental site during a watering event (an asphalt parking lot of $2500m^2$)

293 This study focused on the following variables, all observed in the car park:

- 294 • surface and ground temperature: vertical profile at 0, 1, 2, 3, 4, 5, 6,
295 10, 15, 24, 34, 50 and 75 cm depth;
- 296 • wind speed and direction;
- 297 • convective heat flux;
- 298 • latent heat flux;
- 299 • radiation components.

300 The humidity and air temperature were measured outside from the car park.
301 The experimental devices are presented in Figure 4. The data were collected
302 with a 1 min time step except for the sonic anemometer and the KH20
303 Campbell Sci whose time step were 0.1 s. The final data were averaged to
304 15 min time step.

305 *3.1.2. Description of the watering events*

306 16 watering events (including one natural event - the 15th) were recorded
307 during the entire measurement period (Figure 3). Each of them is described
308 in table 1. During the events numbered 1,2,3 and 6, some technical issues oc-
309 curred and the total volume of water may be different from what is presented
310 in Table 1. For each event, several parameters have been measured:

- 311 • inlet: water temperature, flow, and volume,
- 312 • outlet water temperature, flow, and volume,
- 313 • duration of each watering.

314 An indication is given on the approximate duration of the drying periods.

Watering	Date	Time	Total vol. of water	Intensity	Flow
Number	DD/MM/YY HH:MM	minutes	m^3	mm/m^2	m^3/h
1*	02/06/04 13:42	20	16.96	6.78	43
2*	03/06/04 09:53	20	13.08	5.32	43
3*	03/06/04 15:04	20	15.05	6.02	44
4	04/06/04 08:49	3	2.04	0.81	44
5	04/06/04 11:57	1.5	1.12	0.45	44
6*	04/06/04 13:57	17	14.92	5.97	44
7	07/06/04 08:51	20	13.75	5.50	42
8	07/06/04 13:43	30	21.33	8.53	44
9	08/06/04 09:45	19	12.40	4.96	44
10	08/06/04 15:04	5	3.06	1.22	38
11	09/06/04 09:25	20	14.10	5.64	42
12	09/06/04 13:40	20	16.25	6.50	46
13	09/06/04 15:38	2	1.60	0.64	48
14	10/06/04 08:30	20	15.44	6.18	45
15	10/06/04 12:25	28	2.95	1.18	-
16	11/06/04 08:40	2	1.66	0.67	43

Table 1: Description of each watering event

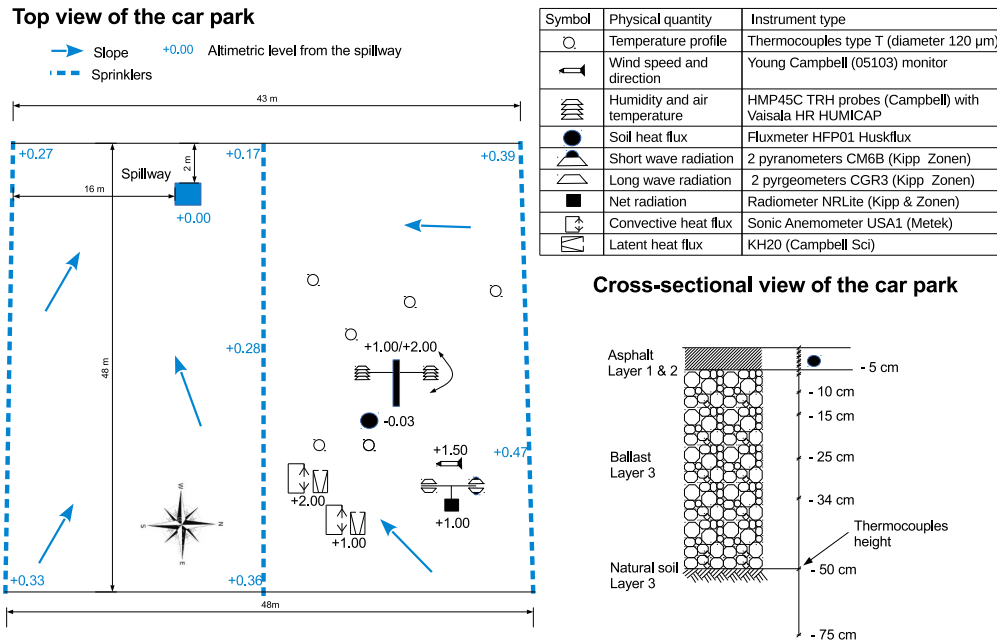


Figure 4: Top view of the car park with instruments approximate location during the campaign and cross-section of the soil composition (see Table 3 for the material properties)

315 *3.1.3. Validation of the model assumptions*

316 It is assumed (sections 2.2.2 and 2.2.4) that energy is exchanged between
 317 the runoff water and the surface only during the first time step ($t=15$ min-
 318 utes). Then the latent heat flux is modelled. Those assumptions are here
 319 verified analysing the temperatures and heat flux measurements.

320 The surface temperature evolution is compared to the water temperature
 321 and flow in the spillway in Figure 5. As soon as the watering event begins
 322 (black line on Figure 5), the surface temperature drops and the water tem-
 323 perature increases (zone 1 on Figure 5) until they reach a balance (dashed
 324 line on Figure 5). A delay of several minutes can be observed between the
 325 temperature signals and the water flow signals (zones 1 and 3 on Figure 5).

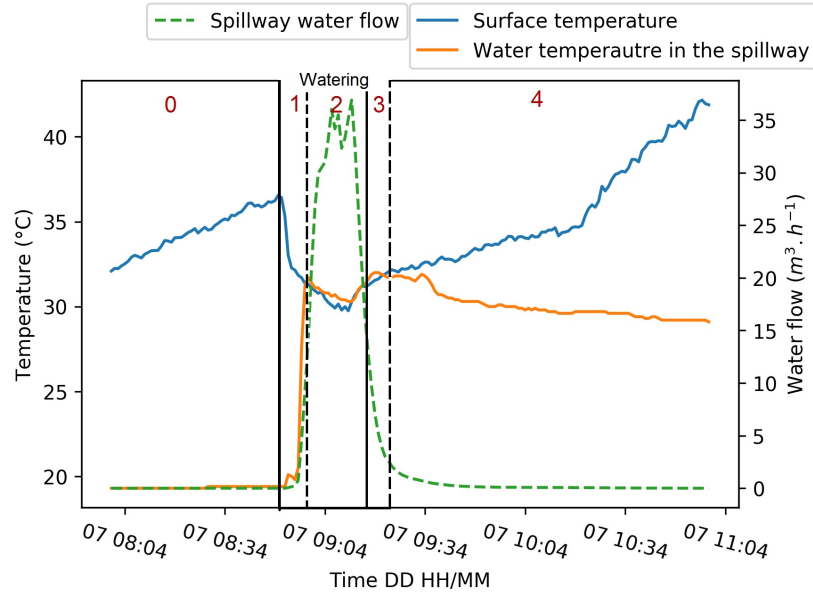


Figure 5: Watering event number 7, June 07th at 08:51am, measured surface temperature in the centre of the parking lot and measured water temperature and water flow in the spillway

326 The thermocouples are located at several meters from the spillway, as it can
 327 be observed in Figure 3. The delay between the different signals is consis-
 328 tent with the water travel time between the thermocouples location and the
 329 spillway. As the balance is reached, both temperatures increase (zone 3):
 330 no more energy is exchanged between the surface and the water layer. The
 331 thermocouples now measures the temperature of the standing water in the
 332 spillway, which slowly decreases (zone 4 on Figure 5).

333 Those observations are compared to the heat fluxes measured presented
 334 in Figure 6. As said before the water temperature reaches very quickly (less
 335 than 20 minutes) the surface temperature (Figure 5) whereas the conductive
 336 heat flux in the ground has a decreasing peak right after watering which then

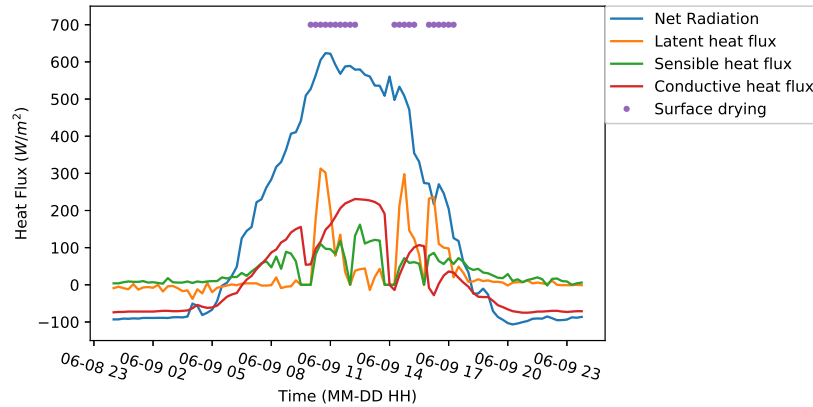


Figure 6: Observed surface energy balance (June 07th)

337 shrink in a short time (about one hour) (Figure 6). Cohard et al (2017 [28])
 338 also noticed a similar trend: the heat flux transferred from the ground to
 339 the water reaches 438 W/m² during a watering event and decreases as soon
 340 as the sprinklers stop (15 minutes). Those observations are consistent with
 341 the assumptions made for our modelling as well as the one used by Herb
 342 et al. (2008 [19]): the runoff convective heat flux exchanged between the
 343 water and the surface can be attributed to the first time step of the watering
 344 event. We assumed that air was saturated during the watering process and
 345 no evaporation occurred immediately. This assumption could not be verified
 346 in this experiment since the latent heat flux sensor was protected when the
 347 sprinklers were working.

348 3.1.4. Water budget

349 When some water is spread over a surface, a fraction runs off whereas
 350 the other fraction is intercepted by the surface until evaporation or infiltra-
 351 tion. The distribution of runoff and pavement storage depends on the surface

352 water-holding capacity, itself related to the surface roughness. This charac-
353 teristic is a parameter of the model that should be set by the user. The
354 purpose of this part is to estimate this parameter through the measurements
355 of the water budget.

356 Cohard et al. (2017 [28]) estimated that for each watering event, the
357 height of water infiltrating the ground does not exceed 0.2 mm. The water
358 left over the surface is thus considered as entirely evaporated. To calculate
359 the corresponding amount, they tested several methods derived from latent
360 heat flux measurement or estimation. Their conclusion is that the latent
361 heat flux estimated according to the SEB method (using measurements for
362 the other fluxes values) was the most accurate. The results fitted with the
363 water budget contrary to the other method used. They were then able to
364 evaluate for each watering event the amount of water evaporated. For events
365 with high volume of water (more than 2 mm), the mean evaporated height
366 is 0.7mm. This value will be used as reference data for the evaluation of the
367 model, and the water holding capacity will be calibrated in the model (see
368 section 3.2.1).

369 *3.2. Comparison between simulation and measurement*

370 The model ability to properly reproduce the physical processes involved
371 during a watering event is evaluated in this section. The model setup used
372 are presented, then the model is evaluated at several depths. Finally, as the
373 soil model is proposed for different optimised grid distributions, the model
374 sensitivity to the node distribution is studied.

Surface energy balance heat flux	Input data used to calculate each flux
Convective heat flux	wind speed air temperature*
Net radiative heat flux	Net radiative flux
Latent heat flux	water height water-holding capacity of the surface air relative humidity* air temperature*
Runoff convective heat flux	water temperature total sprinkled water for each event

*measured outside from the watered zone of the car park

Table 2: Detail of each input data necessary to calculate the upper boundary condition.

375 *3.2.1. Model setup*

376 The simulation is run for the whole period from June 5th, 00:00 to June
377 14th, 00:00, with a time step of 15 minutes. For the soil thermal model, a
378 centimetric grid is used.

379 **Surface energy balance:**

380

381 The heat fluxes are calculated from the observed data presented in Table
382 2. The convective heat flux is calculated from the air temperature and the
383 wind speed. Radiative heat fluxes are the observations. The latent and run-
384 off convective heat fluxes are calculated according to the processing chain
385 presented in Figure 2. The runoff convective heat flux is calculated using
386 the amount of water sprinkled during each watering event derived from the
387 measurement. The temperature of the sprinkled water is set at 18 °C be-
388 fore it reaches the ground. The latent heat flux is calculated from the air
389 characteristics measured outside from the watered zone.

390 **Thermal characteristics:**

391

392 The soil is composed of three different materials: 5 cm-of asphalt, 45 cm-
 393 of ballast and an altered mica-schist natural soil underneath. Soil composi-
 394 tion and thermal properties have not been measured during the experiment.
 395 They have been calibrated according to the observed soil thermal profile,
 396 reducing the difference between the measured and simulated surface temper-
 397 ature, with a centimetric-grid. Data acquired on the 6th of June is used for
 398 calibration. From the measured temperature gradient, changes in the soil
 399 thermal properties within the first layer were identified (0–1 cm, 1–5 cm).

400 Values are gathered in Table 3.

Layer	Material	Depth	Thermal conduc-	Volumetric heat ca-
Number	Characteristics	m	tivity	capacity
			$W.m^{-1}.K^{-1}$	$10^6 J.m^{-3}.K^{-1}$
0	Asphalt Concrete	0.01	2.5	2.3
1	Asphalt Concrete	0.05	2.5	2.1
2	Old Filled Ballast	0.5	1.8	2.3
3	Altered Mica-schist Natural Soil	1	1.3	2.1

Table 3: Calibrated characteristics of the soil

401 **Water-holding capacity:**

402

403 The water storage capacity of the surface may vary a lot depending on
 404 the surface type. To better evaluate this value for our studied area, the
 405 model has been run for two days from the 7th to the 8th of June (4 watering
 406 events), testing the water storage height from 0.3 to 1.4. The effect on the

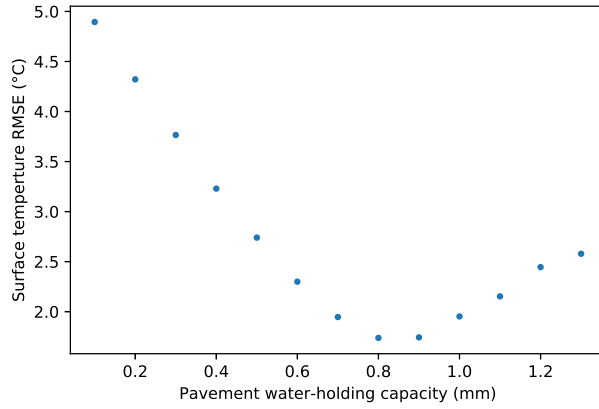


Figure 7: Surface temperature root-mean-square-error (RMSE) as a function of the pavement water-holding capacity (mm) for the calibration period (June, 7th, and 8th)

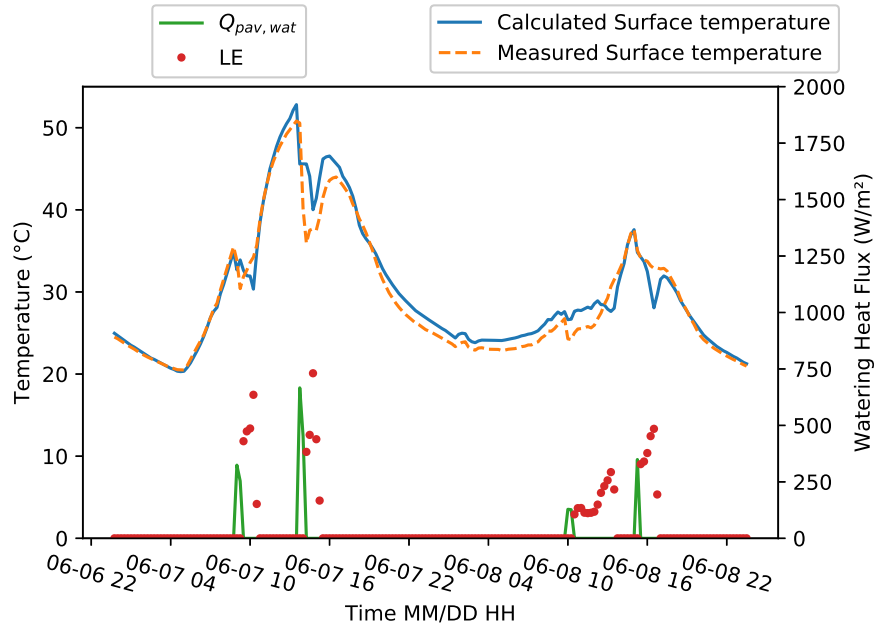


Figure 8: Comparison of simulated and measured temperatures at the surface for the calibration period (June, 7th, and 8th)

407 surface temperature RMSE is shown in Figure 7. A water holding capacity
408 of 0.8 mm minimises the surface temperature RMSE and then is used for
409 the studied car park surface. Figure 8 presents the results of the calibration
410 period and a minimum for a height of 0.8 mm. The temporal variations are
411 well reproduced (there is no phase lag between the signals) except during the
412 watering events.

413 This value is consistent with the mean evaporated height calculated from
414 SEB method for a high amount of water (0.7 mm). In the literature Hendel
415 et al. (2015 [10]) estimate to 1mm the water holding capacity of road surface
416 in the centre of Paris. In TEB the default value is also set to 1 mm (Daniel
417 et al., 2016 [8]).

418 *3.2.2. Watering model evaluation on ROSURE data*

419 The model evaluation is performed by comparing the time series of ob-
420 served and modelled surface temperatures (Figure 9). Temporal variations of
421 the surface temperature are well reproduced (there is no phase lag between
422 the signals) except during the watering events. The same shape is obtained (a
423 decreasing peak followed by more steady period and then an increasing peak)
424 but a lag is observed. This lag might have been attributed to the assumption
425 that the drying stage does not start as long as the sprinklers are in operation.
426 To verify this assumption, we have run some simulations starting the evapo-
427 ration stage while sprinklers were still working. The same time lag was noted
428 and the simulated surface temperature was lower than the observed one or
429 the initial simulation. This lag error could be attributed to the relative hu-
430 midity measurement used for the latent heat flux calculation. The sensor is

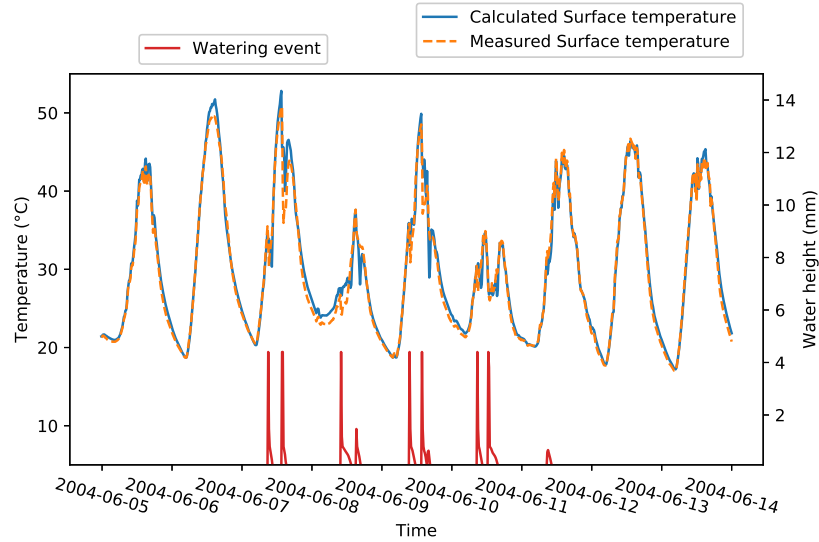


Figure 9: Comparison of simulated and measured temperatures at the surface from June, 5th, to 13th

431 located outside from the sprinkled area and thus potentially underestimates
 432 the real relative humidity of the air in the watered area. This results in an
 433 overestimation of the latent heat flux which may affect the dynamic of the
 434 surface energy balance.

435 In order to determine the overall model performance, the RMSE between
 436 estimated and observed temperatures is calculated at the surface and at
 437 several depths. To estimate the error which may be attributed only to the
 438 watering model, the RMSE is calculated for two different periods. The first
 439 period includes the entire campaign without the calibration days (from June
 440 9th to June 13th), whereas the second includes only two dry days (June 12th
 441 and 13th). The first column assesses the overall model performance (soil
 442 and watering models) while the second indicates the performance relative

Depth	RMSE ($^{\circ}\text{C}$)	RMSE ($^{\circ}\text{C}$)
	From June 8 th 23:45 to the 13 th 23:45 (soil + watering model)	From June 11 th 23:45 and 13 th 23:45 (soil model only)
Surface	1.04	0.71
5 cm	0.86	0.93
10 cm	0.66	0.78
34 cm	0.35	0.46
50 cm	0.21	0.29

Table 4: Evaluation of the centimetric grid watering model according to the experimental data

443 to the soil model only (ability to reproduce heat transfers into the ground).
444 Results are presented in Table 4. The RMSE for the surface temperature
445 is larger when watering events are simulated (1.04 $^{\circ}\text{C}$) than when only the
446 soil model is needed (0.71 $^{\circ}\text{C}$). For this specific data set, the watering model
447 increased the soil model error of 46 %. As the simulated days are not similar
448 (weather condition are varying), this value is only representative for this
449 specific simulation.

450 The assumption was made that the water-holding capacity of the surface
451 was 0.8 mm. As it is an important parameter, the model is also evaluated on
452 its ability to calculate the latent heat flux. For each event, the latent heat
453 fluxes calculated by the model and estimated from the SEB residual method
454 are integrated over each event. The total energy due to evaporation for both
455 methods is compared in Table 5. The relative error stays below 29 %. On
456 average, the model overestimates the latent heat flux by 12 %.

457 The air temperature and the relative humidity used to calculate the evap-

Watering	Date	Duration	Total height of the water layer spread	Latent heat measured from SEB method	Latent heat calculated by the model	Relative error
Number	DD/MM/YY HH:MM	minutes	mm	$10^6 J$	$10^6 J$	%
7	07/06/04 08:51	20	5.50	2.11	1.96	-7.17
8	07/06/04 13:43	30	8.53	2.36	1.96	-17.04
9	08/06/04 09:45	19	4.96	2.00	1.96	-2.12
10	08/06/04 15:04	5	1.22	1.52	1.96	28.71
11	09/06/04 09:25	20	5.64	1.52	1.96	28.79
12	09/06/04 13:40	20	6.50	1.42	1.76	23.77
13	09/06/04 15:38	2	0.64	1.30	1.57	21.07
14	10/06/04 08:30	20	6.18	1.72	1.96	13.66
15	10/06/04 12:25	28	1.18	1.74	1.96	12.60
16	11/06/04 08:40	2	0.66	1.32	1.63	22.88

Table 5: Comparison of the latent heat flux estimated from SEB residue and calculated by the model. For each event, the latent heat fluxes are summed over the event duration.

458 oration were measured outside from the car park. If local parameters were
459 used, an increase of the relative humidity and a decrease of the air temper-
460 ature would have been observed. Then the calculated evaporation heat flux
461 would have been smaller. The use of non-local meteorological data overesti-
462 mates the latent heat flux calculation.

463 3.2.3. Model sensitivity to the discretization

464 In order to reduce the simulation duration while keeping a reasonable
465 accuracy, three node distributions for the soil layer have been proposed in
466 Azam et al. (2017 [17]). They are presented in Figure 10. The sensitivity of
467 the model to the node distribution is here evaluated.

468 Figure 11 compares the surface temperature modelled with the three dif-

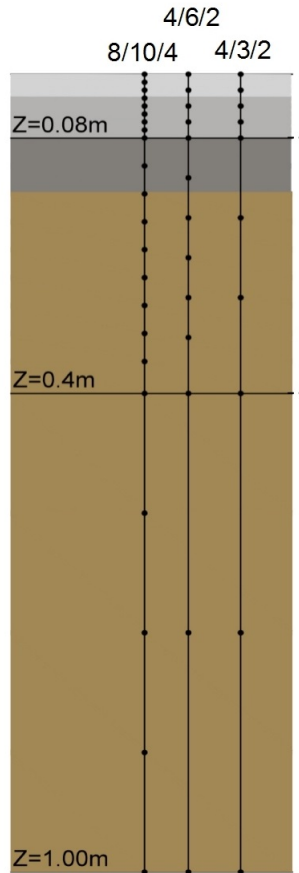


Figure 10: Description of the different grids

469 ferent node distributions with the measured one. Firstly, the three node
 470 distributions allow an accurate modelling of the time series of surface tem-
 471 perature. Nevertheless, the daily maximum peak and minimum trough are
 472 underestimated.

473 The underestimated daily maximum peak and minimum trough are due
 474 to the heat fluxes implementation during watering events. However, the
 475 reduction in the number of nodes deteriorates the results as it leads to dete-

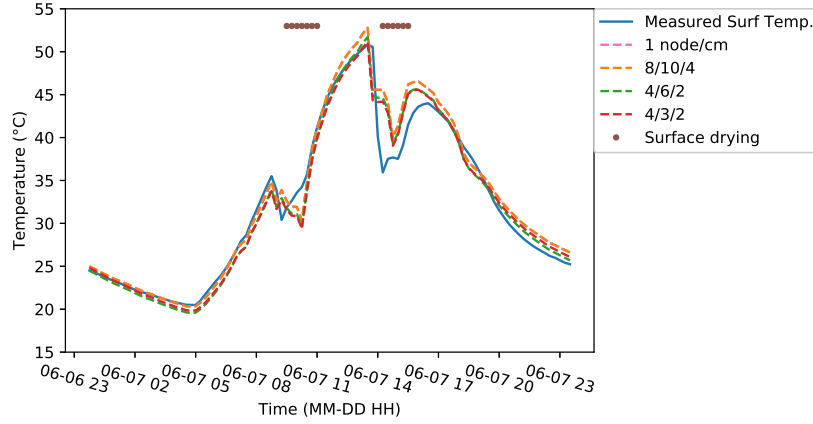


Figure 11: Surface temperature calculated with the different grids compared to that measured (June 7th)

riorate the representation of the heat transfer into the ground. In fact, this induces a time shift of heat conduction, the main influence of which appears when its sign changes.

The RMSE between simulated and observed surface temperatures is calculated for each node distribution (Table 6). The accuracy loss due to the reduction of the number of nodes is also evaluated calculating the RMSE of

Date	Reference data for RMSE calculation	centimetric grid	grid 8/10/4	grid 4/6/2	grid 4/3/2
From June 8 th 23:45 to the 13 th 23:45 (soil + watering model)	observed temperature(°C)	1.04	1.04	1.44	1.50
	simulated temperature using centimetric grid (°C)	-	0.02	1.18	1.21
June 12 th and 13 th (soil model only)	observed temperature (°C)	0.70	0.72	1.10	1.20
	simulated temperature using centimetric grid (°C)	-	0.03	1.14	1.15

Table 6: Evaluation of the model with a reduced number of nodes

482 the simulated surface temperature between each node distribution and the
483 centimetric grid (1 node per cm). The 8/10/4 grid has almost no effect on
484 the simulation performances (the RMSE increase is lower than 4 %). The
485 absolute RMSE increase due to the node distribution is almost similar re-
486 gardless the models used (soil model only or soil model + watering model):
487 0.02, 1.18, and 1.21 °C for grids 8/10/4, 4/6/2 and 4/3/2, respectively. If
488 we report these RMSE to the one due to the model itself (centimetric grid
489 relative to the observed data), the relative accuracy loss due to the nodes
490 distribution is much lower when the water model is taken into consideration.

491 **4. Conclusion**

492 This article focuses on pavement watering as a possible mitigation tech-
493 nique of the UHI effect under heat waves conditions. The literature review
494 revealed that this technique has been mainly studied through experimen-
495 tal works. To the best of our knowledge, the impact of pavement watering
496 on urban energy balance at the micro-scale has not yet been addressed by
497 modelling.

498 The main purpose of this article was to implement a watering model
499 within an urban micro-scale model (SOLENE-Microclimat) and to evaluate
500 it according to a field experiment.

501 The watering model was elaborated on a literature review and evaluated
502 on an open asphalt car park. Two fluxes were taken into account: the runoff
503 convective heat flux (exchanged between the surface and the runoff water)
504 and the latent heat flux. The runoff convective heat flux is often neglected

505 by existing models at meso-scale whereas the high difference of temperature
506 between surface and the water spread makes it prevailing under heat wave
507 conditions. In the case of the experiment used to evaluate the model, the
508 modelled heat flux represents 20 % of the overall cooling flux ($Q_{wat-pav} + LE$)
509 due to the pavement watering.

510 The latent heat flux is limited by the water holding capacity of the pave-
511 ment. This important parameter has been estimated using two methods: one
512 based on simulation and the other based on the observation. The results are
513 almost similar: the water holding capacity of the studied pavement is about
514 0.8 mm, comparable to the 1 mm height found in the literature. The esti-
515 mated latent heat flux is in average 12 % higher than the observed one. The
516 relative error never exceeds 30 %. An explanation of this overestimation is
517 that the relative humidity data used for the latent heat flux calculation was
518 probably lower than the reality (the sensor was located outside the watered
519 area).

520 The global accuracy of the model was evaluated using the temperature
521 observed at the surface and at several depths. The absolute RMSE for the
522 surface temperature is larger when watering events are simulated (1.04 °C)
523 than under dry conditions when only the soil model is used (0.71 °C).

524 The sensitivity of the model to the node distribution has finally been
525 studied. Three soil model node distributions were compared. The 8/10/4
526 grid has almost no effect on the simulation performances (the RMSE increase
527 is lower than 4 %).

528 This paper provides a detail evaluation of the watering model perfor-
529 mances when compared with experimental data. This model can be used
530 to assess the cooling induced by pavement watering mitigation technique at
531 micro-scale, which was not possible until now. The impact on local comfort
532 could then be estimated.

533 The efficiency of watering techniques is constrained by the surface po-
534 tential evaporation which depends directly on the surface holding capacity.
535 The model could then be used to optimise the watering scenario according
536 to the surface characteristics of streets. The impact of different materials on
537 microclimat model could then be compared.

538 **Acknowledgements**

539 This research work was carried out within the scope of the EVA Project,
540 funded by the ADEME (French Environment and Energy Management Agency)
541 under contract no. 1216C0037 and conducted in collaboration with Veolia
542 2EI. The authors are grateful to the ADEME for its financial support, as
543 well as to IFSTTAR, LHEEA, and ONEVU for providing us with the exper-
544 imental data.

545 **References**

- 546 [1] J.-M. Robine, S. L. K. Cheung, S. Le Roy, H. Van Oyen, C. Griffiths, J.-
547 P. Michel, F. R. Herrmann, Death toll exceeded 70,000 in europe during
548 the summer of 2003, *Comptes rendus biologies* 331 (2008) 171–178.

- 549 [2] K. Laaidi, A. Zeghnoun, B. Dousset, P. Bretin, S. Vandentorren, E. Gi-
550 raudet, P. Beaudeau, The impact of heat islands on mortality in paris
551 during the august 2003 heat wave, *Environmental health perspectives*
552 120 (2012) 254.
- 553 [3] S. Conti, P. Meli, G. Minelli, R. Solimini, V. Toccaceli, M. Vichi, C. Bel-
554 trano, L. Perini, Epidemiologic study of mortality during the summer
555 2003 heat wave in italy, *Environmental research* 98 (2005) 390–399.
- 556 [4] M. Santamouris, L. Ding, F. Fiorito, P. Oldfield, P. Osmond, R. Paolini,
557 D. Prasad, A. Synnefa, Passive and active cooling for the outdoor built
558 environment—analysis and assessment of the cooling potential of mitiga-
559 tion technologies using performance data from 220 large scale projects,
560 *Solar Energy* (2016).
- 561 [5] M. A. Hendel, M. Colombert, Y. Diab, L. Royon, Measurement of the
562 cooling efficiency of pavement-watering as an urban heat island mitiga-
563 tion technique, *Journal of Sustainable Development of Energy, Water*
564 *and Environment Systems* 3 (2015) 1–11.
- 565 [6] S. Himeno, R. Takahashi, A. Asakura, K. Koike, S. Fujita, Using snow
566 melting pipes to verify the water sprinkling s effect over a wide area,
567 *NOVATECH 2010* (2010).
- 568 [7] X. Yang, L. Zhao, Diurnal thermal behavior of pavements, vegetation,
569 and water pond in a hot-humid city, *Buildings* 6 (2015) 2.
- 570 [8] M. Daniel, A. Lemonsu, V. Viguié, Role of watering practices in large-

- 571 scale urban planning strategies to face the heat-wave risk in future cli-
572 mate, *Urban Climate* (2016).
- 573 [9] A. M. Broadbent, A. M. Coutts, N. J. Tapper, M. Demuzere, The cooling
574 effect of irrigation on urban microclimate during heatwave conditions,
575 *Urban Climate* (2017).
- 576 [10] M. Hendel, M. Colombert, Y. Diab, L. Royon, An analysis of pave-
577 ment heat flux to optimize the water efficiency of a pavement-watering
578 method, *Applied Thermal Engineering* 78 (2015) 658–669.
- 579 [11] S. Grossman-Clarke, J. A. Zehnder, T. Loridan, C. S. B. Grimmond,
580 Contribution of land use changes to near-surface air temperatures during
581 recent summer extreme heat events in the phoenix metropolitan area,
582 *Journal of Applied Meteorology and Climatology* 49 (2010) 1649–1664.
- 583 [12] C. Grimmond, M. Blackett, M. Best, J. Barlow, J. Baik, S. Belcher,
584 S. Bohnenstengel, I. Calmet, F. Chen, A. Dandou, et al., The inter-
585 national urban energy balance models comparison project: first results
586 from phase 1, *Journal of applied meteorology and climatology* 49 (2010)
587 1268–1292.
- 588 [13] V. Masson, A physically-based scheme for the urban energy budget in
589 atmospheric models, *Boundary-layer meteorology* 94 (2000) 357–397.
- 590 [14] L. Malys, Évaluation des impacts directs et indirects des façades et des
591 toitures végétales sur le comportement thermique des bâtiments, Ph.D.
592 thesis, École nationale supérieure d’architecture (Nantes), 2012.

- 593 [15] M. Musy, L. Malys, B. Morille, C. Inard, The use of solene-microclimat
594 model to assess adaptation strategies at the district scale, *Urban Climate*
595 14 (2015) 213–223.
- 596 [16] J. Bouyer, Modelisation et simulation des microclimats urbains-Etude de
597 l’impact de l’amenagement urbain sur les consommations energetiques
598 des batiments, Ph.D. thesis, Universite de Nantes, 2009.
- 599 [17] M.-H. Azam, B. Morille, J. Bernard, M. Musy, F. Rodriguez, A new
600 urban soil model for solene-microclimat: Review, sensitivity analysis
601 and validation on a car park, *Urban Climate* (2017).
- 602 [18] S. Dupont, P. G. Mestayer, E. Guilloteau, E. Berthier, H. Andrieu,
603 Parameterization of the urban water budget with the submesoscale soil
604 model, *Journal of Applied Meteorology and Climatology* 45 (2006) 624–
605 648.
- 606 [19] W. R. Herb, B. Janke, O. Mohseni, H. G. Stefan, Ground surface tem-
607 perature simulation for different land covers, *Journal of Hydrology* 356
608 (2008) 327–343.
- 609 [20] V. Singh, C. Xu, Evaluation and generalization of 13 mass-transfer equa-
610 tions for determining free water evaporation, *Hydrological Processes* 11
611 (1997) 311–323.
- 612 [21] C.-Y. Xu, V. Singh, Evaluation and generalization of temperature-based
613 methods for calculating evaporation, *Hydrological processes* 15 (2001)
614 305–319.

- 615 [22] T. Asaeda, V. T. Ca, The subsurface transport of heat and moisture
616 and its effect on the environment: a numerical model, *Boundary-Layer*
617 *Meteorology* 65 (1993) 159–179.
- 618 [23] Z. Qin, P. Berliner, A. Karnieli, Numerical solution of a complete surface
619 energy balance model for simulation of heat fluxes and surface tempera-
620 ture under bare soil environment, *Applied mathematics and computa-*
621 *tion* 130 (2002) 171–200.
- 622 [24] H. Saito, J. Simunek, Effects of meteorological models on the solution of
623 the surface energy balance and soil temperature variations in bare soils,
624 *Journal of Hydrology* 373 (2009) 545–561.
- 625 [25] M. Best, A model to predict surface temperatures, *Boundary-Layer*
626 *Meteorology* 88 (1998) 279–306.
- 627 [26] G. Mihalakakou, M. Santamouris, J. Lewis, D. Asimakopoulos, On the
628 application of the energy balance equation to predict ground tempera-
629 ture profiles, *Solar Energy* 60 (1997) 181–190.
- 630 [27] O. A. Alduchov, R. E. Eskridge, Improved magnus form approximation
631 of saturation vapor pressure, *Journal of Applied Meteorology* 35 (1996)
632 601–609.
- 633 [28] J. Cohard, J. Rosant, F. Rodriguez, H. Andrieu, P. Mestayer, P. Guille-
634 vic, Energy and water budgets of asphalt concrete pavement under
635 simulated rain events, *Urban Climate* (2017).